Progress In Electromagnetics Research B, Vol. 20, 187–203, 2010

A DIVERGENCE-FREE BEM TO MODEL QUASI-STATIC CURRENTS: APPLICATION TO MRI COIL DESIGN

C. C. Sanchez, S. G. Garcia, L. D. Angulo, C. M. de Jong and A. R. Bretones

Department of Electromagnetism
University of Granada
Fuentenueva s/n, Granada 18071, Spain

Abstract—The modeling of quasi-static optimization problems often involves divergence-free surface current densities. In this paper, a novel technique to implement these currents by using the boundary element method framework is presented. A locally-based characterization of the current density is employed, to render a fully geometry-independent formulation, so that it can be applied to arbitrary shapes. To illustrate the versatility of this approach, we employ it for the design of gradient coils for MRI, providing a solid mathematical framework for this type of problem.

1. INTRODUCTION

Many problems in engineering require to determine the spatial distribution of electric currents flowing in a conductive surface which satisfies given requirements for the fields, electromagnetic energy, etc. they produce. The reconstruction of current distribution on the conducting surface subjected to these constraints can be seen as an inverse problem. An appropriate and realistic formulation of this type of problems is presented in this paper, by incorporating a suitable model of the current under search, in terms of the stream function, into the Boundary Element Method (BEM).

The use of stream function for the characterization of surface current densities has been widely employed [1]. The BEM has been proved to be an excellent tool in the solution of electromagnetic problems [2, 3]; and the incorporation of the stream function into a numerical computational technique, such us BEM, has also been already considered for the solution of electromagnetic inverse

Corresponding author: C. C. Sanchez (ccobos@ugr.es).

problems [4]. A relevant application of this topic is the design of gradient coils for magnetic resonance imaging (MRI). MRI is a non-invasive medical technique, which relies on the use of well defined and controlled magnetic fields, with given gradients to encode spatially the signals from the sample. These field gradients are generated by wire coils usually placed on cylindrical surfaces (although other coil geometries [5, 6] or even permanent magnet can be also employed [7]).

The problem in gradient coil design is to find optimal positions for the multiple windings of coils so as to produce fields with the desired spatial dependence and properties [5] (low inductance, high gradient to current ratio, minimal resistance, and good field gradient uniformity). Hence coil design is then an electromagnetic inverse problem which can be formulated as a constrained optimization, for which the inverse BEM method has been successfully employed [8, 9]. Stream-function based current models for coil design were proposed in [10], though only valid up to second-order since the current became non-divergent for higher orders. A formulation for quasi-static electromagnetic topological optimization problems involving good conductors for simple quadrilateral meshes can also be found in [4].

In this paper, we present a novel technique to model a quasi-static current density over a given conducting surface for optimization problems. This approach relies on the BEM mathematical framework, as the boundary of the conducting surface is discretized into triangular patches, on which the involved magnitudes are approximated and solved keeping the divergence-free nature up to arbitrary order. We characterize the current through the stream function, given in terms of specific functions locally based, so that the resulting formulation is completely geometry-independent, and can be applied to any current-carrying surface. To demonstrate the power and versatility of our method, we provide an overview of the design of a cylindrical transverse gradient coil for MRI applications. Numerical examples of the coil performance are presented to demonstrate the efficiency of the proposed technique for solving this type of inverse problems.

Although application of our method is illustrated with design of gradient coil for MRI, it is aimed to be a general approach well suited for any electromagnetic inverse problems under low-frequency conditions or applications where a linear or quadratic functional, such as the energy or dissipation, has to be optimized. This technique can also be formulated for any order of element; here it is illustrated for linear and quadratic interpolation.

2. FUNDAMENTALS

2.1. Stream Function: BEM Formulation

An electric current density, $\mathbf{J}$, flowing on PEC surface must satisfy two main conditions

i) $\mathbf{J}$ must flow on the coil surface. That is

$$\mathbf{J} \cdot \mathbf{n} = 0. \tag{1}$$

where $\mathbf{n}$ is the local unit surface vector.

ii) The current density, $\mathbf{J}$, must be divergence-free [11]

$$\nabla \cdot \mathbf{J} = 0, \tag{2}$$

so that it obeys the continuity equation over the coil surface in the quasi-static domain.

Since $\mathbf{J}$ is a divergence-free vector, it can be expressed as the curl of another vector perpendicular to the surface where the current flows

$$\mathbf{J}(\mathbf{r}) = \nabla \times \left[\varphi(\mathbf{r})\ \mathbf{n}(\mathbf{r})\right], \tag{3}$$

where $\mathbf{n}(\mathbf{r})$ is a unit vector normal to the surface, and φ is usually referred to as the stream function [9].

BEM requires the discretization of the bounding surfaces into surface elements. Let us assume that the surface, S, on which we want to find the optimal current, is divided into T triangular elements (not necessarily flat)

$$S = \bigcup_{t=1}^{T} S_t \tag{4}$$

with N nodes, $\{\mathbf{r}_n\}_{n=1}^{N}$, lying at each vertex of the element (and at the mid-point of each side for quadratic curved elements and extra points for higher elements [12]).

Let us now define

N2T, which maps the nth-node, $\mathbf{r}_n$ to the set of elements

$$N2T(\mathbf{r}_n) = \{S_{ni}\}_{i=1}^{\Omega} \tag{5}$$

where Ω is the number of elements for which $\mathbf{r}_n$ is a node.

T2N, which maps a given element, S_t with its nodes

$$T2N(S_t) = \{\mathbf{r}_{ti}\}_{i=1}^{\Lambda} \tag{6}$$

where Λ is the number of nodes in the element.

Finally, we will define the shape functions [12, 13] to express the position of a point placed at one element, $\mathbf{r} \in S_t$, in terms of the coordinates of the nodes of this element, $T2N(S_t) = \{\mathbf{r}_{ti}\}_{i=1}^{\Lambda}$

$$\mathbf{r} = \sum_{i}^{\Lambda} \mathbf{r}_{ti} N^{ti}(\mathbf{r}). \tag{7}$$

Each shape function, N^{ti}, is associated with one node $\mathbf{r}^{ti}$, and it must satisfy a interpolation condition: It takes the unit value when evaluated at this node and is zero at the other nodes

$$N^{ti}(\mathbf{r}_{tj}) = \delta_{i,j}. \tag{8}$$

These shape functions can also be employed to expand the functions defined within the element in terms of their nodal values

$$\varphi(\mathbf{r}) = \sum_{i}^{\Lambda} \varphi_{ti} N^{ti}(\mathbf{r}) \tag{9}$$

where $\varphi_{ti} = \varphi(\mathbf{r}_{ti})$. It bears noting that the interpolations used to describe the geometry and the variation of the function with the space (and hence the shape function used to describe each of them) can be different for a given element. For instance, we can consider shape functions of first order to represent the geometry (six-node flat element), and second-order shape functions to describe φ on the element. Isoparametric representations arise when the order of both interpolations are the same.

Let us denote the nodal values at of the stream function used to express current density on the surface (3) by I_n

$$\varphi(\mathbf{r}_n) = I_n, \qquad \forall n = 1, \ldots, N. \tag{10}$$

The value of the stream function for a given point $\mathbf{r}$ in the tth-element, $\mathbf{r} \in S_t$ can be expressed as a linear combination of the nodal values of the element where the point is located

$$\varphi(\mathbf{r}) = \sum_{i=1}^{\Lambda} N_t^{ti}(\mathbf{r}) I_{ti}. \tag{11}$$

The above sum can also be expressed as a sum over all the nodes

$$\varphi(\mathbf{r}) = \sum_{n=1}^{N} \mathcal{N}^n(\mathbf{r}) I_n \tag{12}$$

by defining a generalized function $\mathcal{N}^n$ related to the nth-node

$$\mathcal{N}^n(\mathbf{r}) = \begin{cases} 0 & \text{if } \mathbf{r}_n \notin S_t \\ N_t^n(\mathbf{r}) & \text{if } \mathbf{r}_n \in S_t \end{cases} \tag{13}$$

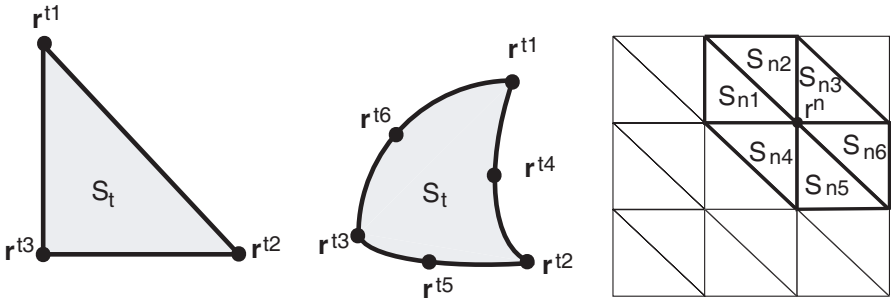

Figure 1. (a) $T2N(S_t)$ for a linear flat element ($\Lambda = 3$); (b) $T2N(S_t)$ for a quadratic element ($\Lambda = 6$). The $N2T(\mathbf{r}_n)$ function relates a given node $\mathbf{r}_n$ with the elements to which it belongs; (c) flat linear elements.

and $N_t^n(\mathbf{r})$ is the shape function associated to the same node $\mathbf{r}_n$ in the element S_t. According to the definition above, for any $\mathbf{r}$

$$\mathcal{N}^n(\mathbf{r}) = 0, \quad \text{unless} \quad \mathbf{r} \in \{S_{ni}\}_{i=1}^{\Omega} = N2T(\mathbf{r}_n). \tag{14}$$

Also it should be stressed that although I_n is a fixed value for a given node, the function $N_t^n(\mathbf{r})$ associated to the nth-node, *depends on the element in which* $\mathbf{r}$ *lies*.

In order for the current to be stationary no net flux should flow into or out the conducting surface. Thus a common value of the stream function for all nodes belonging to the same edge on the boundary, must be enforced. The stream function so defined is continuous, and can be replaced into Eq. (3) to find the current density as

$$\mathbf{J}(\mathbf{r}) = \sum_{n=1}^{N} I_n \nabla \times [\mathcal{N}^n(\mathbf{r})\ \mathbf{n}(\mathbf{r})]. \tag{15}$$

If we introduce the *current basis vector* associated to the nth-node as

$$\boldsymbol{\jmath}^n(\mathbf{r}) = \nabla \times [\mathcal{N}^n(\mathbf{r})\ \mathbf{n}(\mathbf{r})], \tag{16}$$

then

$$\mathbf{J}(\mathbf{r}) = \sum_{n=1}^{N} I_n\ \boldsymbol{\jmath}^n(\mathbf{r}), \tag{17}$$

where

$$\boldsymbol{\jmath}^n(\mathbf{r}) = \begin{cases} 0 & \text{if } \mathbf{r}_n \notin S_t \\ \nabla \times [N_t^n(\mathbf{r})\ \mathbf{n}(\mathbf{r})] & \text{if } \mathbf{r}_n \in S_t \end{cases} \tag{18}$$

so that

$$\boldsymbol{\jmath}^n(\mathbf{r}) = 0, \quad \text{unless} \quad \mathbf{r} \in N2T(\mathbf{r}_n). \tag{19}$$

Note that $\boldsymbol{\jmath}^n(\mathbf{r})$ varies depending on the element in which $\mathbf{r}$ lies. The set of all possible values that $\boldsymbol{\jmath}^n(\mathbf{r})$ can take in its associated elements $N2T(\mathbf{r}_n) = \{S_{ni}\}_{i=1}^{\Omega}$, is termed the **current element** (Fig. 2(b)).

This current density satisfies the required conditions specified in Eqs. (1)–(2). It is seen clearly that $\mathbf{J}$ lies on the surface and also it is straightforwardly divergence-free

$$\nabla \cdot \mathbf{J}(\mathbf{r}) = \sum_{n=1}^{N} I_n \, \nabla \cdot \boldsymbol{\jmath}^n(\mathbf{r}) = 0 \tag{20}$$

since

$$\nabla \cdot \boldsymbol{\jmath}^n(\mathbf{r}) = \nabla \cdot \Big[\nabla \times [\mathcal{N}^n(\mathbf{r}) \; \mathbf{n}(\mathbf{r})]\Big] = 0. \tag{21}$$

The current density at $\mathbf{r}$ can be equivalently defined in terms of a linear combination of the basis function associated to the element where $\mathbf{r}$ lies (Fig. 2(a)), where the weights are the stream function's nodal values

$$\mathbf{J}(\mathbf{r}) = \sum_{i=1}^{\Lambda} I_{ti} \, \boldsymbol{\jmath}^{ti}(\mathbf{r}). \tag{22}$$

Although Eq. (22), provides a simple expression for the current, Eq. (17) is the employed for the numerical implementations of this paper, as it presents a more convenient form for optimization purposes.

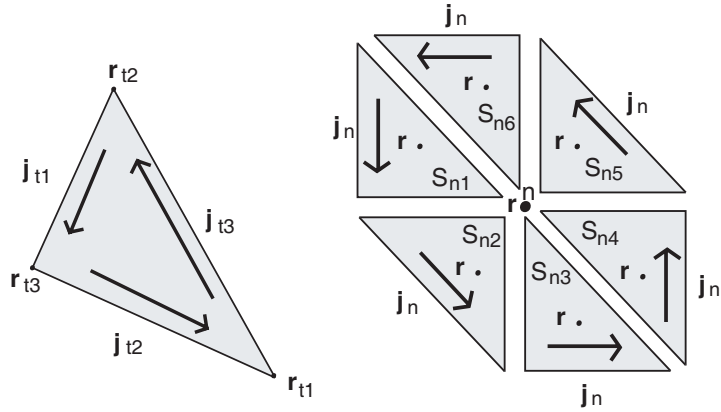

Figure 2. (a) Current basis vectors in one flat element; (b) current basis vector associated to the nth-node $\boldsymbol{\jmath}^n(\mathbf{r})$ (its value depends on the particular element which $\mathbf{r}$ lies in).

2.2. Current Basis in Generalized Coordinates

The current basis vectors are found by computation of the curl of the shape functions. Let assume a non-orthogonal coordinate system [15], locally defined at each element, by three axis with tangential vectors in the directions of the ξ or η, plus and the outward direction normal to the surface element (Fig. 3).

The components of the curl are given by [14]

$$[\nabla \times [N^n(\xi,\eta)\ \mathbf{n}(\xi,\eta)]]_\xi = \sqrt{\frac{g_{11}}{g}}\left[\frac{\partial(N^n(\xi,\eta)/\sqrt{g^{33}})}{\partial\eta}\right] \tag{23}$$

$$[\nabla \times [N^n(\xi,\eta)\ \mathbf{n}(\xi,\eta)]]_\eta = -\sqrt{\frac{g_{22}}{g}}\left[\frac{\partial(N^n(\xi,\eta)/\sqrt{g^{33}})}{\partial\xi}\right] \tag{24}$$

where g is the determinant of the metric, and

$$g_{ij} = \sum_{k=1}^{3} \frac{\partial x^k}{\partial \xi^i}\frac{\partial x^k}{\partial \xi^j} \tag{25}$$

The following notation has been used $x^1 = x$, $x^2 = y$ and $x^3 = z$ for cartesian; $\xi^1 = \xi$, $\xi^2 = \eta$ and ξ^3 for the normal coordinate in the parametric space. The metric tensor which can be written as

$$\overline{\overline{g}} = \begin{pmatrix} \boldsymbol{\xi}\cdot\boldsymbol{\xi} & \boldsymbol{\xi}\cdot\boldsymbol{\eta} & 0 \\ \boldsymbol{\eta}\cdot\boldsymbol{\xi} & \boldsymbol{\eta}\cdot\boldsymbol{\eta} & 0 \\ 0 & 0 & 1 \end{pmatrix} \tag{26}$$

where

$$\boldsymbol{\xi} = \frac{\partial \mathbf{r}}{\partial \xi}; \qquad \boldsymbol{\eta} = \frac{\partial \mathbf{r}}{\partial \eta}. \tag{27}$$

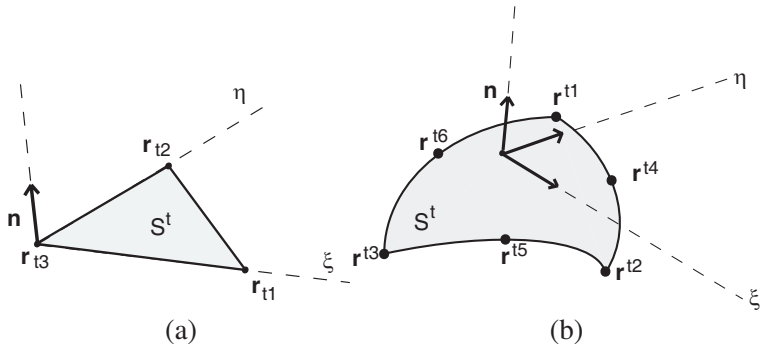

Figure 3. Coordinates system (ξ, η) for (a) flat elements and (b) quadratic curved element.

Therefore according to Eqs. (23)–(24), the current basis $\boldsymbol{\jmath}^{ti}$ are easily obtained if the metric and the derivatives of the shape functions are knowns. Let us illustrate this result with examples of the current associated with different variations of φ within the elements.

For flat elements

$$\boldsymbol{\xi} = \mathbf{r}_{t1} - \mathbf{r}_{t3}; \qquad \boldsymbol{\eta} = \mathbf{r}_{t2} - \mathbf{r}_{t3}. \tag{28}$$

and

$$g^{1/2} = 2A. \tag{29}$$

where A is the area of the element. The complete calculation of the basis making use of the derivative of the shape functions is found in Appendix A.

If we consider an isoparametric linear approximation the $\boldsymbol{\jmath}^{ti}$ are (see Fig. 2(a))

$$\begin{aligned} \boldsymbol{\jmath}^{t1} &= -\frac{(\mathbf{r}_{t2} - \mathbf{r}_{t3})}{2A}; \qquad \boldsymbol{\jmath}^{t2} = \frac{(\mathbf{r}_{t1} - \mathbf{r}_{t3})}{2A}; \\ \boldsymbol{\jmath}^{t3} &= \frac{(\mathbf{r}_{t2} - \mathbf{r}_{t3})}{2A} - \frac{(\mathbf{r}_{t1} - \mathbf{r}_{t3})}{2A}. \end{aligned} \tag{30}$$

It should be mentioned that the use of isoparametric linear representation leads to a constant current over the element, as expected, since the current is described by one order less than the stream function approximation. In addition, we can see that this result is equivalent to Pissanetzky's [8] local description of the current.

Next we consider linear elements and quadratic shape functions for the stream function description over the element. So as in the foregoing case we are dealing with linear flat elements. But this time to describe a quadratic behavior of φ within the element we use second order shape functions ($\Lambda = 6$, see Appendix A). Therefore although we only need the three triangle vertices to describe the geometry, to represent a quadratically varying stream function the mid-points must also be considered producing a six-node flat triangle. To compute the current basis, we evaluate the curl of the shape functions of the second order that describe the stream function. The current basis functions are thus[†]

$$\boldsymbol{\jmath}^{t1}(\xi,\eta) = -(4\xi - 1)\frac{(\mathbf{r}_{t2} - \mathbf{r}_{t3})}{2A}; \tag{31}$$

$$\boldsymbol{\jmath}^{t2}(\xi,\eta) = (4\eta - 1)\frac{(\mathbf{r}_{t1} - \mathbf{r}_{t3})}{2A}; \tag{32}$$

$$\boldsymbol{\jmath}^{t3}(\xi,\eta) = (1 - 4\zeta)\left[\frac{(\mathbf{r}_{t1} - \mathbf{r}_{t3})}{2A} - \frac{(\mathbf{r}_{t2} - \mathbf{r}_{t3})}{2A}\right]; \tag{33}$$

[†] A proof of the divergence free condition of these function can be easily given in the parametric space: $\nabla_{\xi,\eta} \cdot \boldsymbol{\jmath}^{ti}(\xi,\eta) = 0$.

$$\boldsymbol{J}^{t4}(\xi,\eta) = 4\xi\frac{(\mathbf{r}_{t1}-\mathbf{r}_{t3})}{2A} - 4\eta\frac{(\mathbf{r}_{t2}-\mathbf{r}_{t3})}{2A}; \quad (34)$$

$$\boldsymbol{J}^{t5}(\xi,\eta) = 4(\zeta-\eta)\frac{(\mathbf{r}_{t1}-\mathbf{r}_{t3})}{2A} + 4\eta\frac{(\mathbf{r}_{t2}-\mathbf{r}_{t3})}{2A}; \quad (35)$$

$$\boldsymbol{J}^{t6}(\xi,\eta) = -4\xi\frac{(\mathbf{r}_{t1}-\mathbf{r}_{t3})}{2A} - 4(\zeta-\xi)\frac{(\mathbf{r}_{t2}-\mathbf{r}_{t3})}{2A}. \quad (36)$$

Analogously in the case of a isoparametric quadratic formulation BEM, the current basis vectors can be computed by using the derivatives of the shape functions employed in the previous case, although a different metric must be used, which can be easily found from the tangential vectors $\boldsymbol{\xi}$ and $\boldsymbol{\eta}$ for quadratic curved elements

$$\boldsymbol{\xi} = \frac{\partial\mathbf{r}}{\partial\xi} = (4\xi-1)\mathbf{r}_1 + (1-4\zeta)\mathbf{r}_3 + 4\eta\mathbf{r}_4 - 4\eta\mathbf{r}_5 + 4(\zeta-\xi)\mathbf{r}_6 \quad (37)$$

$$\boldsymbol{\eta} = \frac{\partial\mathbf{r}}{\partial\eta} = (4\eta-1)\mathbf{r}_2 + (1-4\zeta)\mathbf{r}_3 + 4\xi\mathbf{r}_4 + 4(\zeta-\eta)\mathbf{r}_5 - 4\xi\mathbf{r}_6 \quad (38)$$

3. NUMERICAL APPLICATION: DESIGN OF MRI GRADIENT COILS

In this section we apply the above described method to the design of a cylindrical gradient coil for MRI. The goal is to find an optimal current distribution over a given conducting surface so as to achieve a desired magnetic field in a region of interest (ROI), to balance the torque experienced [‡] by the current density in an applied static magnetic field and to minimize the magnetic stored energy.

In our case, a cylindrical surface is considered, with a radius of 0.5 m and a length of 2 m, on which we need to calculate the surface currents, which create a target field in the ROI with a linear variation of B_z along x, and a gradient strength $G = 1\,\mathrm{Tm}^{-1}$. The desired ROI for gradient uniformity is taken as a uniform distribution of 400 points spread over a sphere of radius 0.18 m. (Fig. 4).

According to these requirements we can define the following quadratic programming (QP) problem [16], in which a quadratic function (or Lagrangian) of several variables, which are subject to linear constraints, must be minimized

$$\mathcal{F} = \frac{1}{2}\sum_{k=1}^{K}[B_z(\mathbf{r}_k) - B_{des,z}]^2 + \alpha W_{magn} \quad (39)$$

[‡] For the sake of clarity the torque term is omitted in the following formulation, as geometries with axial symmetry will experience no net torque in the presence of a z-directed field.

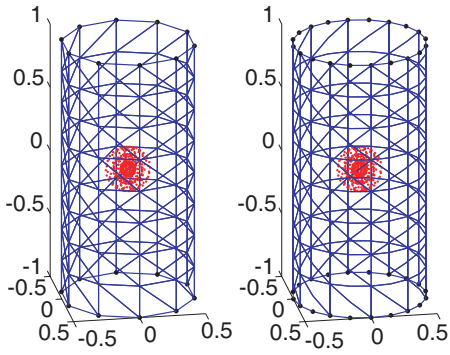

Figure 4. Cylinder meshed using (a) 160 flat elements (b) and using 160 quadratic curved elements. The ROI is formed from a spherical distribution of 400 points (in red) at the centre of the figure; and the nodes at the edges are marked in black.

here $B_{des,z}$ is the z-component of the desired field over a set of K points in the ROI. B_z is the actual field, α is the weight for the the magnetic energy, W_{magn}.

The coefficient α can be interpreted as a regularization parameter, which is chosen so that the magnetic field deviates by less than a given value, $\Delta B_z(\mathbf{r}) \leq 5\%$ over the ROI. This parameter, then, allows control of the coil properties, and illustrates the trade-off between coil features. The coefficient α can also be seen as a regularization parameter [17, 18].

Now the current-carrying surface has to be meshed into T triangular elements S_t with N nodes, $\{\mathbf{r}_n\}_{n=1}^{N}$. Applying the divergence-free current technique previously described, we find the discretized versions of the functions involved in the problem.

For instance, the B_z produced by the current distribution can be expressed as

$$B_z(\mathbf{r}) = \sum_{n=1}^{N} I_n b_z^n(\mathbf{r}), \tag{40}$$

where b_z^n is the z-component of the magnetic induction produced by the current element associated to the nth-node

$$b_z^n(\mathbf{r}) = \frac{\mu_0}{4\pi} \sum_{i=1}^{\Omega} \int_{S_{ni}} \frac{j_y^n(\mathbf{r}')(x - x') - j_x^n(\mathbf{r}')(y - y')}{|\mathbf{r} - \mathbf{r}'|^3} \, dS'. \tag{41}$$

The coefficient $b_z^n(\mathbf{r})$ includes integrals that usually cannot be solved analytically, so a numerical integration procedure has to be adopted. As the field point, $\mathbf{r}$, is never at the surface, the integrals

involved are non-singular and can be easily computed using Gaussian quadrature [13].

Analogously the magnetic energy in the coil can be written as

$$W_{mag} = \frac{\mu_0}{8\pi} \int_S \int_{S'} \frac{\mathbf{J}(\mathbf{r})\mathbf{J}(\mathbf{r}')}{|\mathbf{r}-\mathbf{r}'|} dSdS' = \frac{1}{2} \sum_{n=1}^{N} \sum_{m=1}^{N} I_n I_m L_{mn} \tag{42}$$

where L_{mn} is the mutual inductance between the mth and nth current elements

$$L_{mn} = \frac{\mu_0}{4\pi} \sum_{i=1}^{\Omega} \sum_{j=1}^{\Omega} \int_{S_{ni}} \int_{S_{mj}} \frac{\boldsymbol{\jmath}^n(\mathbf{r}) \cdot \boldsymbol{\jmath}^m(\mathbf{r}')}{|\mathbf{r}-\mathbf{r}'|} \, dSdS'. \tag{43}$$

The double integral involved in the definition of the components, L_{mn}, of the inductance matrix shows a singular behavior when $m = n$. Analytical expressions for these singular double integrals have been presented in [21] for linear isoparametric elements, although a general approach for dealing with these type of double weak singular integrals is given in [22]. This is based on a transformation into a local polar coordinate system where the integration can be performed by avoiding the singularity.

The incorporation of the discretized versions of the functions into the problem, leads to the functional $\mathcal{F}(\mathbf{I})$ (39), where $\mathbf{I} = (I_1, I_2, \ldots, I_N)$ are the set of the stream function nodal values. The function $\mathcal{F}(\mathbf{I})$ can now be minimized by finding the parameters which make

$$\frac{\partial \mathcal{F}(I)}{\partial I_p} = 0; \qquad p = 1, \ldots, N. \tag{44}$$

and so we obtain the optimal stream function values that minimize the functional.

The inverse problem finishes with the identification of the optimal nodal values of the stream function, which allow us to construct the discretized version of the current density over the surface, that produces the desired field variation and satisfies the other imposed constraints. However, the final goal in coil design is to find the wire arrangement that approximates the continuous current distribution. The conversion of the current solution into a conductor pattern is achieved by contouring the stream function [19, 20].

4. RESULTS

A transverse coil has been designed with the proposed model by using an isoparametric quadratic interpolation. Fig. 5 shows the stream-function, for the X-gradient coil plot over the cylindrical surface

geometry, and how the wires of the gradient coil are obtained by contouring the stream function (red wires indicate reversed current flow with respect to blue). These wire arrangements when energized produce the B_z field displayed in Fig. 6. Field magnitudes were calculated using the elemental Biot-Savart expression applied directly

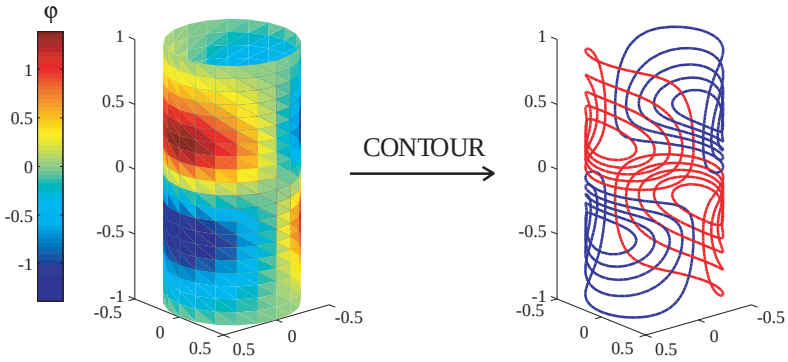

Figure 5. Stream function over the coil surface and wire arrangement (stream lines). Note that φ is normalized to unity since its scale is unimportant for contouring purposes. We choose a number of contour levels $N_c = 10$ that are equally spaced [4] (Brideson et al. [19] proved that equally spaced contours of φ give an approximation to $\mathbf{J}$).

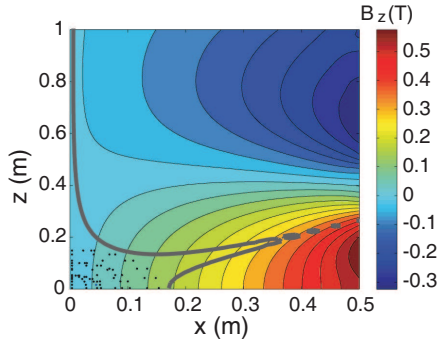

Figure 6. Contours of the B_z field produced by the wire arrangement Fig. 5. The grey line delineates the region where the field deviates by less than 5% from linearity. The points where the field is evaluated in the ROI are shown in black. The target field employed is $B_z(r) = G_x x$, where the gradient proportionality constant has been considered as $G_x = 1\,\mathrm{T/m}$. The current intensity carried by the coil to produced this field is then $I = 24.53\,\mathrm{kA}$.

to the wire paths. Integrating also over the wire-paths the torque experienced by the coil can also be found. For this example it is less than $10^{-6}\,\mathrm{NmA^{-1}T^{-1}}$. Using FastHenry © [23], a multipole impedance extraction tool, and assuming the coil wires have a 3 mm diameter, the value of the inductance is found to be 235 µH for this case, which yields the following performance parameter (FOM) [5]

$$\frac{\eta^2}{L} = 9.6 \times 10^{-6}\ T^2 m^{-2} A^{-2} H^{-1}. \tag{45}$$

4.1. Study of the Convergence

The coil design problem presented can be tackled by application of any of the different order of approximation in BEM that were illustrated in the Section 2.2. The efficacy of employing curved rather than flat element geometry and linear rather than parabolic approximation of the stream function over the element is now explored by performing a mesh convergence study, that is, we study the solutions of every BEM approximation for different mesh densities (number of elements). We applied this study to the design of cylindrical transverse and longitudinal gradient coils, where the radius of the coil cylinder was 0.40 m and its total length 1.60 m.

Figure 7(a) shows that the quadratic (red line) and linear (blue line) isoparametric solutions converge to the same value for the simple problem of a cylindrical transverse gradient coil. The convergence for the case of flat triangles with a parabolic stream function (green line), is faster than in the other two cases. Fig. 7(b) displays another convergence plot in terms of the FOM for a longitudinal gradient coil. The parabolic isoparametric approximation exhibits a higher rate of convergence with increasing number of elements, that is, convergence occurs for a smaller number of elements. It is worth noting that for the two previous cases, there seems to be a residual error between the convergence of solutions using flat elements and curved elements.

For both problems, all the BEM approximations produce effective solutions and a finer mesh results in a more accurate solution. The particular BEM approximation for which convergence occurs at the smallest number of elements will depend on the particular problem. However, as a mesh is made finer, the computation time increases as shown in Fig. 7(c). As expected the computation time grows with the number of elements and is always higher for curved triangles and parabolic interpolations.

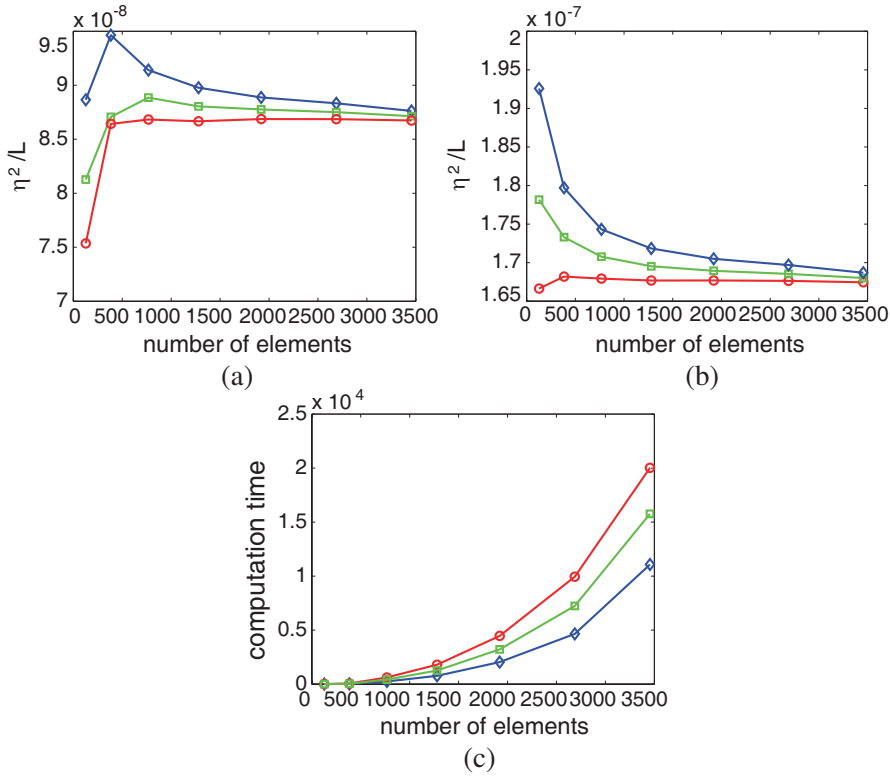

Figure 7. (a) Convergence study in terms of the FOM ($a^{-5}T^2m^{-2}A^{-2}H^{-1}$) for a cylindrical transverse gradient coil (height = 1.6 m and radius = 0.4 m), the linear and quadratic isoparametric solutions are shown in blue (diamond marker) and red (circle marker) respectively. The green line (square marker) displays the solution for flat elements with quadratic evolution of φ; (b) convergence study for a cylindrical longitudinal gradient coil of similar geometry; (c) computation time for different numbers of surface elements.

5. CONCLUSION

A new technique to model realistic quasi-static currents has been proposed and evaluated. The method provides a new framework for solving inverse electromagnetic problems, it can be seen as an inverse boundary element method which is geometry-independent and so it can be applied a wide variety of shapes and geometries.

The current can be reconstructed with any order of interpolation, as it is locally characterized in each mesh element through a set of

vectors (current basis) that can be related to the curl of the shape functions used to describe the variation of the stream function.

Here it has been evaluated for gradient coil design, allowing the production of efficient torque-balanced coils of minimum inductance.

APPENDIX A. SHAPE FUNCTIONS

This Appendix provides the first and second order shape functions and their derivatives in parametric coordinates.

A.1. Linear Shape Functions

The first order shape functions are

$$N^1(\xi,\eta)=\xi; \qquad N^2(\xi,\eta)=\eta; \qquad N^3(\xi,\eta)=1-\eta-\xi. \tag{A1}$$

with $\xi,\eta\in[0,1]$.

Derivatives of the shape functions

$$\begin{aligned} &\frac{\partial N^1(\xi,\eta)}{\partial\xi}=1; \qquad \frac{\partial N^2(\xi,\eta)}{\partial\xi}=0; \qquad \frac{\partial N^3(\xi,\eta)}{\partial\xi}=-1;\\ &\frac{\partial N^1(\xi,\eta)}{\partial\eta}=0; \qquad \frac{\partial N^2(\xi,\eta)}{\partial\eta}=1; \qquad \frac{\partial N^3(\xi,\eta)}{\partial\eta}=-1 \end{aligned} \tag{A2}$$

A.2. Quadratic Shape Functions

Second order shape functions, ($\Lambda=6$), in the parametric space are given by

$$\begin{aligned} N^1(\xi,\eta)&=\xi(2\xi-1); \qquad N^4(\xi,\eta)=4\xi\eta;\\ N^2(\xi,\eta)&=\eta(2\eta-1); \qquad N^5(\xi,\eta)=4\zeta\eta;\\ N^3(\xi,\eta)&=\zeta(2\zeta-1); \qquad N^6(\xi,\eta)=4\xi\zeta, \end{aligned} \tag{A3}$$

where $\zeta=1-\eta-\xi$, and $\xi,\eta\in[0,1]$.

Derivatives of the shape functions

$$\begin{aligned} &\frac{\partial N^1(\xi,\eta)}{\partial\xi}=4\xi-1; \quad \frac{\partial N^2(\xi,\eta)}{\partial\xi}=0; \qquad \frac{\partial N^3(\xi,\eta)}{\partial\xi}=1-4\zeta;\\ &\frac{\partial N^4(\xi,\eta)}{\partial\xi}=4\eta; \quad \frac{\partial N^5(\xi,\eta)}{\partial\xi}=-4\eta; \qquad \frac{\partial N^6(\xi,\eta)}{\partial\xi}=4(\zeta-\xi)\\ &\frac{\partial N^1(\xi,\eta)}{\partial\eta}=0; \quad \frac{\partial N^2(\xi,\eta)}{\partial\eta}=4\eta-1; \qquad \frac{\partial N^3(\xi,\eta)}{\partial\eta}=1-4\zeta;\\ &\frac{\partial N^4(\xi,\eta)}{\partial\eta}=4\xi; \qquad \frac{\partial N^5(\xi,\eta)}{\partial\eta}=4(\zeta-\eta); \quad \frac{\partial N^6(\xi,\eta)}{\partial\eta}=-4\xi \end{aligned} \tag{A4}$$

ACKNOWLEDGMENT

The work described in this paper has received funding from the European Community's Seventh Framework Programme FP7/2007-2013, under grant agreement No. 205294 (HIRF SE project), and from the Spanish National Projects TEC2007-66698-C04-02, CSD2008-00068, DEX-530000-2008-105, and the Junta de Andalucia Project TIC1541.

REFERENCES

1. Bandelier, B., C. Daveau, P. Haghi Ashtiani, A. Rais, and F. Rioux-Damidau, "Use of stream functions for the computation of currents in thin circuits determination of the impedances," *IEEE Transactions on Magnetics*, Vol. 36, No. 4, 760–764, 2000.
2. Zacharopoulos, A., S. Arridge, O. Dorn, V. Kolehmainen, and J. Sikora, "3D shape reconstruction in optical tomography using spherical harmonics and BEM," *PIERS Online*, Vol. 2, No. 1, 48–52, 2006.
3. Ruan, B. and Y. Wang, "New topography inversion using EM field," *Progress In Electromagnetics Research*, Vol. 1, No. 1, 79–83, 2005.
4. Peeren, G. N., "Stream function approach for determining optimal surface currents," *Journal of Computational Physics*, Vol. 191, No. 1, 305–321, 2003.
5. Turner, R., "Gradient coil design: A review of methods," *Magn. Reson. Imaging*, Vol. 11, 903–920, 1993.
6. Li, X., D. Xie, and J. Wang, "A novel target field method for designing uniplanar self-shield gradient coils of fully open MRI device," *Journal of Electromagnetic Waves and Applications*, Vol. 21, No. 12, 1635–1644, 2007.
7. Hong, L. and D. Zu, "Shimming permanent magnet of MRI scanner," *Progress In Electromagnetics Research Symposium*, Vol. 3, No. 6, 859–864, 2007.
8. Pissanetzky, S., "Minimum energy MRI gradient coil of general geometry," *Measurement of Science Technology*, Vol. 3, 667–673, 1992.
9. Lemdiasov, R. A. and R. Ludwig, "A stream function method for gradient coil design," *Concepts in Magnetic Resonance Part B: Magnetic Resonance Engineering*, Vol. 26B, No. 1, 67–80, 2005.
10. Marin, L., H. Power, R. W. Bowtell, C. Cobos Sanchez, A. A. Becker, P. Glover, and I. A. Jones, "Boundary element method for an inverse problem in magnetic resonance imaging

gradient coils," *Computer Methods in Engineering & Sciences*, 2007.

11. Jackson, J. D., *Classical Electrodynamics*, Wiley, New York, 1962.
12. París, F. and J. Cañas, *Boundary Element Method: Fundamentals and Applications*, Oxford Science Publications, 1997.
13. Brebbia, C. A., J. F. C. Telles, and L. C. Wrobel, *Boundary Element Techniques*, Springer-Verlag, 1984.
14. Holland, R., "Finite-difference solution of Maxwell's equations in generalized nonorthogonal coordinates," *IEEE Trans. Nucl. Sci.*, Vol. NS-30, 4586–4591, 1983.
15. Pozrikidis, C., *A Practical Guide to Boundary-element Methods with the Software Library BEMLIB*, Chapman & Hall/CRC, 2002.
16. Gill, P. E., W. Murray, and M. H. Wright, *Practical Optimization*, Academic Press, London, 1981.
17. Tiknonov, A. N. and V. Y. Arsenin, *Methods for Solving Ill-posed Problems*, Nauka, Moscow, 1986.
18. Goharian, M., M. Soleimani, and G. R. Moran, "A trust region subproblem for 3D electrical impedance tomography inverse problem using experimental data," *Progress In Electromagnetics Research*, Vol. 94, 19–32, 2009.
19. Brideson, M. A., L. K. Forbes, and S. Crozier. "Determining complicated winding patterns for shim coils using stream functions and the target-field method," *Concepts in Magnetic Resonance*, Vol. 14, No. 1, 9–18, 2002.
20. Qi, F., X. Tang, Z. Jin, L. Wang, D. Zu, and W. Wang, "A new target field method for optimizing longitudinal gradient coils' property," *Progress In Electromagnetics Research Symposium*, Vol. 3, No. 6, 865–869, 2007.
21. Eibert, T. F. and V. Hansen, "On the calculation of potential integrals for linear source distributions on triangular domains," *IEEE Transactions on Antennas and Propagation*, Vol. 43, No. 12, 1499–1502, 1995.
22. Marin, L., H. Power, R. W. Bowtell, C. Cobos Sanchez, A. A. Becker, P. Glover, and I. A. Jones, "Numerical solution for an inverse MRI problem using a regularized boundary element method," *(Special Issue) Engineering Analysis with Boundary Elements*, 2007.
23. Kamon, M., M. J. Tsuk, and J. K. White, "Fasthenry: A multipole-accelerated 3-D inductance extraction program," *IEEE Transactions on Microwave Theory and Techniques*, Vol. 42, 1750–1758, 1994.